Molecular-Scale Understanding of the Embrittlement in Polyethylene Ocean Debris

Christopher Garvey, Marianne Impéror-Clerc, Stéphan Rouzière, Gwenaël Gouadec, Olivier Boyron, Laura Rowenczyk, Anne-Françoise Mingotaud, Alexandra A. ter Halle

Molecular scale understanding of the embrittlement in polyethylene ocean debris

Christopher J. Garvey[1,2,3,4]†, Marianne Impéror-Clerc,[1] Stéphan Rouzière,[1] Gwenaël Gouadec,[5] Olivier Boyron,[6] Laura Rowenczyk,[7] Anne Françoise Mingotaud[7] and Alexandra ter Halle[7*]*

1. Laboratoire de Physique des Solides, UMR 8502, CNRS, Université Paris Saclay, France.

2. Lund Institute for Advanced Neutron and X-ray Scattering, Lund, Sweden.

3. Biofilm—Research Center for Biointerfaces and Biomedical Science Department, Faculty of Health and Society, Malmö University, Malmö, Sweden

4. Australian Nuclear Science and Technology Organisation, Locked Bag 2001, Kirrawee DC, NSW 2232, Australia.

5. Sorbonne Université, CNRS, Laboratoire MONARIS, c49, F75252, Paris, France.

6. C2P2 - LCPP Group, UMR CNRS 5265, Université de Lyon, ESCPE Lyon, Bat 308F, 43 Bd du 11 novembre 1918, 69616 Villeurbanne, France.

7. Laboratoire des IMRCP, Université de Toulouse, CNRS UMR 5623, Université Paul Sabatier, 118, route de Narbonne, F-31062 Toulouse Cedex 09, France.

KEYWORDS

polymer, plastics, polyethylene, weathering, X-ray scattering, Raman spectroscopy, differential scanning calorimetry, size exclusion chromatography

ABSTRACT

The fate of plastic waste is a pressing issue since it forms a visible and long-lived reminder of the environmental impact of consumer habits. In this study we examine the structural changes in the lamellar arrangements of semi-crystalline polyethylene (PE) packaging waste with an aim to understand the physical mechanisms of embrittlement in PE exposed to the marine environment. PE microplastics and macroplastics from identifiable PE packaging were collected in the Atlantic Ocean and compared to new PE boxes. Several experimental techniques interrogate the effects of environmental exposure on their bulk and surface properties. Size exclusion chromatography determines the molecular weight distribution of the PE polymer chains and differential scanning calorimetry gives the crystallinity. Small and wide angles X-ray scattering examines the packing of PE chains into semi-crystalline lamellae. Longitudinal acoustic mode Raman spectroscopy provides a complementary measurement on the length of PE polymer chains extending through the crystalline lamellar domains. The overall picture at the molecular scale is that although PE becomes more crystalline with environmental exposure, the lamellar order present in new packing boxes, is disrupted by the weathering process. This process has important implications for embrittlement and subsequent degradation.

39

40 TOC Abstract Art

41

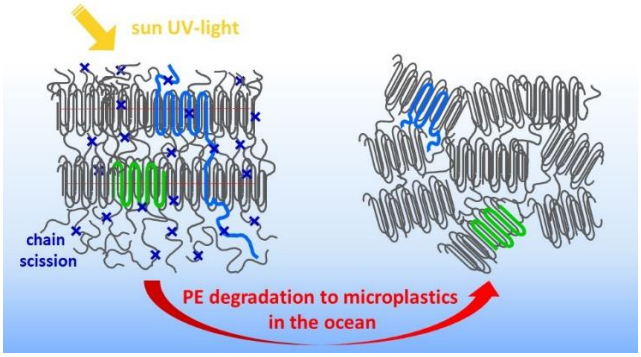

42

43

INTRODUCTION

In recently past decades consumer habits have changed the dominant packaging material deposited into the biosphere.[1, 2] Polyethylene, and more generally polyolefins, are produced extremely efficiently on an industrial scale and have become the first choice for low cost single use barrier materials. This usage was once dominated by cellulose, had well-defined pathways for the degradation and metabolic utilisation by the biosphere of the glucose monomer; such pathways for polyethylene are limited.[3] As a result the environmental load of polyethylene waste steadily increases with little incorporation into the biosphere.[1, 2] In this study we consider the physico-chemical transformations of an important thermoplastic, polyethylene, under the influence of prolonged environmental exposure, drifting in the ocean.

The conceptual framework for organisation of polyethylene in packaging[4], and understanding the subsequent nanostructural changes due to environmental exposure are outlined in Fig. 1. Physically, this structure represents the competition between the energetically favourable crystallisation process and its kinetic limitation by the entanglement of the long extended polymer chains which span the amorphous regions and could enter the a given lamellae more than once.[4] There is a kinetic arrest of the crystallisation process started from the melt[4] and so the degree of crystallisation for packaging materials is a strong function of the processing conditions (thermal history and shear) and initial starting material (molecular weight and chain branching). Previously we have shown that exposure to UV light causes growth of the crystalline lamellae through progressive release of the kinetic constraints via chain scission.[5, 6] This physical transformation, increasing crystallinity, has been shown to immediately influence the mechanical stability of the

material (embrittlement)[6] but also the permeability of the polyethylene to oxygen and subsequent chemical reaction/degradation.

Here we combine several experimental approaches that provide complementary perspectives on selected PE samples, going from original PE packaging, to weathered macroplastics (>20 mm) and weathered microplastics (1 to 5 mm - Tables SI-1 and SI-2). The objective is to obtain a deeper understanding of the nano-structural evolution of the PE materials during environmental exposure, especially the evolution of the lamellar organisation. First, differential scanning calorimetry (DSC) and size exclusion chromatography (SEC) provide information on the kinetic arrest process; DSC by providing the crystallinity (with no assumption on the crystallite morphology) and SEC by the indication of the molecular weight distribution of the constituent polymer chains. Wide angle X-ray scattering (WAXS) provides, again, an experimental perspective on the crystallinity of the materials, and results are compared to those obtained from DSC. Furthermore, since WAXS is sensitive to the packing of the PE chains inside the crystalline lamellae, it gives a measure of the coherence length along specific crystallographic directions - D_{110}/D_{200} - of the crystalline arrangement of the PE chains (Fig. 1).

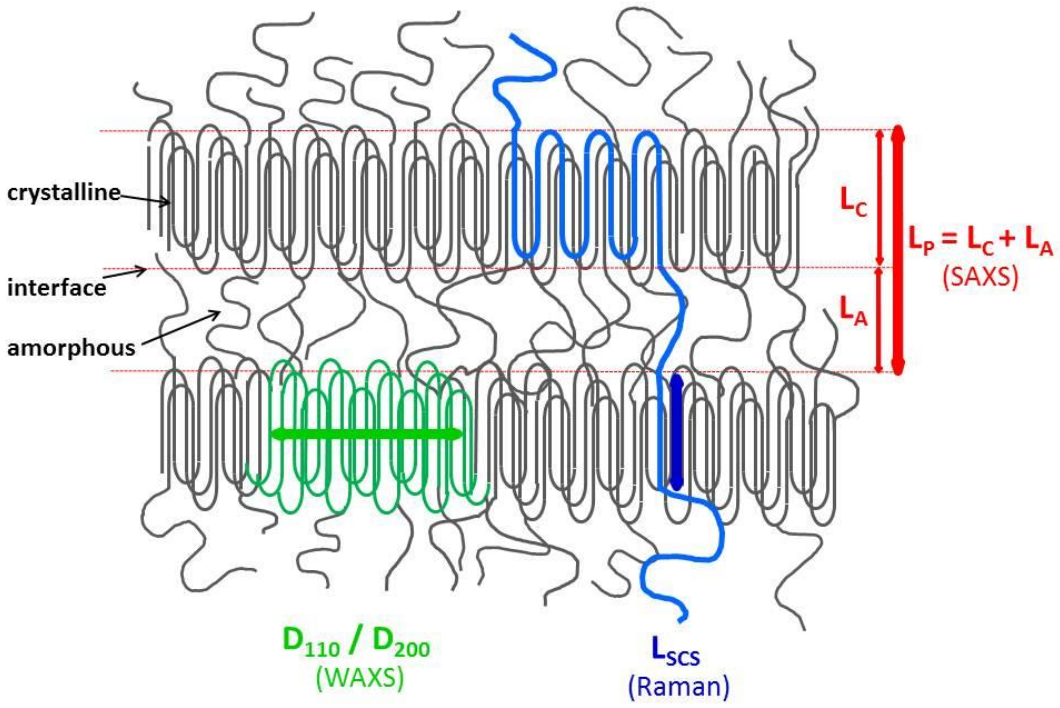

Fig. 1: The semi-crystalline lamellar model for PE. The individual chain highlighted in blue spans both crystalline and amorphous regions and extends over several crystalline lamellae. The long period L_P (measured by SAXS) is the distance between adjacent crystalline lamellae; L_p is the sum of the lamella thickness (L_C) and the extension of the amorphous sub-region (L_A). The crystalline order is characterized by WAXS through the coherence lengths (in green). Inside crystalline lamellae, polymer chains are all parallel to each other. They may also be slightly tilted but for simplicity, the Figure is drawn without a tilt angle. The straight chain segment length L_{SCS} is measured by Raman spectroscopy across the crystalline lamellae. Note that L_{SCS} and L_C may be slightly different (see text).

The nanoscale organisation of PE is probed by combining small angle X-ray scattering (SAXS) and Raman spectroscopy. A peak in the SAXS measurements gives direct evidence of the lamellar semicrystalline organisation[4] and the characteristic distances in the lamellar structure (Fig. 1; the long period L_P is the sum of a crystalline lamella thickness L_C and of the amorphous sub-region extension L_A; the linear crystallinity, linC, is defined by the ratio $linC = L_C/L_P$). Longitudinal acoustic mode (LAM) Raman measurements are sensitive to L_{SCS}, the length of the straight

polyethylene chain segments inserted through the lamellae (Fig. 1). Values of L_C and L_{SCS} are always very close, but not exactly identical, as will be discussed afterwards. For example, a tilt angle (typically 35°, following literature data [7-10]) of the polymer chains may be present inside the crystalline lamellae, depending on the way the PE samples were prepared. However, in Figure 1, for simplicity, the semi-crystalline organisation is depicted with no tilt angle. Values of L_C and L_{SCS} are compared with the caveat that X-ray scattering probes the bulk organisation of the PE chains in the volume of the transmitted X-ray beam (about 1 mm^3), whereas Raman spectroscopy is probing smaller volumes (a few μm^3) at the surface of the sample.

MATERIALS AND METHODS

SAMPLE COLLECTION

Macroplastics and microplastics were collected from the Guyavoile sailing vessel in the accumulation area of the North Atlantic subtropical gyre, in May 2014 and June 2015, during the "7th Continent" French expedition.[11] Macroplastics were visible from the boat and floated on the sea surface. Microplastics were collected using a manta net (mesh size 300 μm). Details of how the debris were collected, sorted out and stored are described elsewhere.[11] All the sample's collection details and labelling are given in Tables SI-1 and SI-2. Some samples were not analysed by the full suite of techniques due to limited amount of sample.

SIZE EXCLUSION CHROMATOGRAPHY AND DIFFERENTIAL SCANNING CALORIMETRY (DSC)

High temperature SEC and DSC analyses were used to analyse the molecular weight distribution and crystallinity of PE samples, respectively. The experimental practice and analysis have been discussed elsewhere[12] and are detailed in the Supplementary Information (SI).

X-RAY SCATTERING

X-ray scattering involves the measurement of the scattered intensity at a defined angle relative to the incident X-ray beam, θ. The scattered intensity, I, is expressed as a function of the scattering vector, q, defined by:

$$q = 4\pi . sin(\theta/2)/\lambda \quad (1)$$

,where λ is the wavelength of the incident radiation. WAXS and SAXS measurements, which differ in the range of scattering vectors considered, were both performed on a homebuilt instrument (Laboratoire de Physique des Solides, Université Paris-Sud, France) operating with monochromatic copper radiation ($\lambda_{CuK\alpha}$ = 0.1542 nm) delivered to the sample by a multilayer W/Si optics coupled with a rotating anode generator (Rigaku HU3R, 40kV-40mA).

WAXS images were recorded on a sensitive image plate detector MAR345 (marXperts, Hamburg, Germany) with a pixel size of 0.150 mm^2, placed at a distance of 100 mm from the sample. Acquisition time for each measurement was 300 s. WAXS 1-D diagrams were obtained by radial integration of the intensity of each image. The analysis and processing of the 1-D WAXS data in terms of coherence length of the D_{110} and D_{200} crystallographic planes and fractional crystallinity are detailed in the SI.

2D SAXS images were acquired on a two-dimensional Pilatus 200K detector (Dectris, Baden, Switzerland) using a sample to detector distance of 1236 mm. The gaps between detector modules were eliminated by combining 2 images with slight positional offsets. The size of the X-ray beam on the sample was 0.8 x 0.8 mm^2. The data was reduced to the radially averaged intensity versus q form, I(q), using the measurement geometry, a pixel size of 0.172 mm^2 and a background subtraction of the empty beam in air, scaled by the sample transmission using the NIKA macros[13] written for IgorPro (Wavemetrics, Oswego, USA). The final q-range was $0.094 < q < 1.64$ nm^{-1}.

RAMAN SPECTROSCOPY

In semi-crystalline polymers, the Straight Chain Segments length L_{SCS} can be approximated from the position of Raman first-order Longitudinal Acoustic Mode (σ_{LAM}) using Mizushima–Simanouti equation[14, 15]:

$$L_{SCS} = \frac{1}{2c\sigma_{LAM}\sqrt{\frac{\rho}{E}}} \quad (2)$$

In Eq. (2), ρ is the density of the crystallites, E their Young's modulus and c is the speed of light. In this study we shall use ρ = 972 kg.m^{-3} (the experimental density of PE single crystals[16]) and E = 305 GPa (Young's modulus in the direction of "all-trans" PE chains in interaction). [17-20] Eq. (2) pairs one unique σ_L wavenumber with each L_{SCS} value and the experimental spectrum $I_{LAM}(\sigma_L)$ is classically converted into a Lamellar Thickness Distribution (LTD) using Eq. (3) [21] (see details in the SI) where the $\left(1 - e^{-\frac{hc}{kT}\sigma_L}\right)$ term is the thermal population factor from Maxwell-Boltzmann statistics:

$$N(L_{SCS}) \propto I_{LAM}(\sigma_L) \times \left(1 - e^{\frac{-hc}{kT}\sigma_L}\right) \times \sigma_L^2 \quad (3)$$

Samuel and Hamagushi[22] recently introduced a correction factor in Eq. (3) but discarding it makes no difference for our samples, as discussed in the SI.

All spectra were recorded in backscattering mode using the 514.5 nm line of an Innova 90C-6UV Ar^+ ion laser (Coherent) and a LabRam HR 800 Raman spectrometer equipped with an Ultra Low Frequency (ULF) module for Rayleigh scattering filtration (Horiba Jobin Yvon). A minimum of five spectra were recorded for each sample. Depending on the signal to noise ratio, either the most intense one or the average one was fitted, after correction of the ULF-induced distortion

through a procedure described in the SI. Further details on the experimental setup, the probed volume, fluorescence quenching and peak fitting procedures may also be found in the SI.

STATISTICAL ANALYSIS

Statistical tests were performed on the full set of data. A Fisher test was first performed to compare the variances of the samples before applying a Student's t-test if appropriate. Owing to the low number of macro samples, Fisher's test failed in some cases. Mann Whitney tests were then performed considering non-parametric data. The corresponding indications are reported in the Figures.

RESULTS AND DISCUSSION

The focus is the nanostructural evolution of PE, crystallization, in several types of original packaging and weathered samples. Firstly, we assess the differences between commercial packaging samples (Nesquik and Folgers boxes, code names Ne and Fo) and the corresponding weathered macroplastics (w-Ne and w-Fo). Secondly, these macroplastics are compared to several microplastics of unknown origin. Because of the much smaller physical dimensions of the latter (see Table SI 1), it is assumed that they have been weathered for a longer time, and have therefore reached a more advanced oxidation state.[12] However, because the history of the samples (before they were collected) and the starting material are not well defined, the conditions of formation of the debris are largely unknown. Secondly, owing to the small number of microplastics presented here (10), statistical tests were systematically performed to compare with original packaging and the paired macro-plastics.

SIZE EXCLUSION CHROMATOGRAPHY

SEC was performed to determine the molecular weight distribution of the polymer chains. Typical SEC profiles are shown in Figure SI 1. The cumulative weight fractions obtained from the analysis are shown in Fig. 2. The analysis is elaborated in Table SI 3. Samples D19 and C8 did not have sufficient material for the analysis.

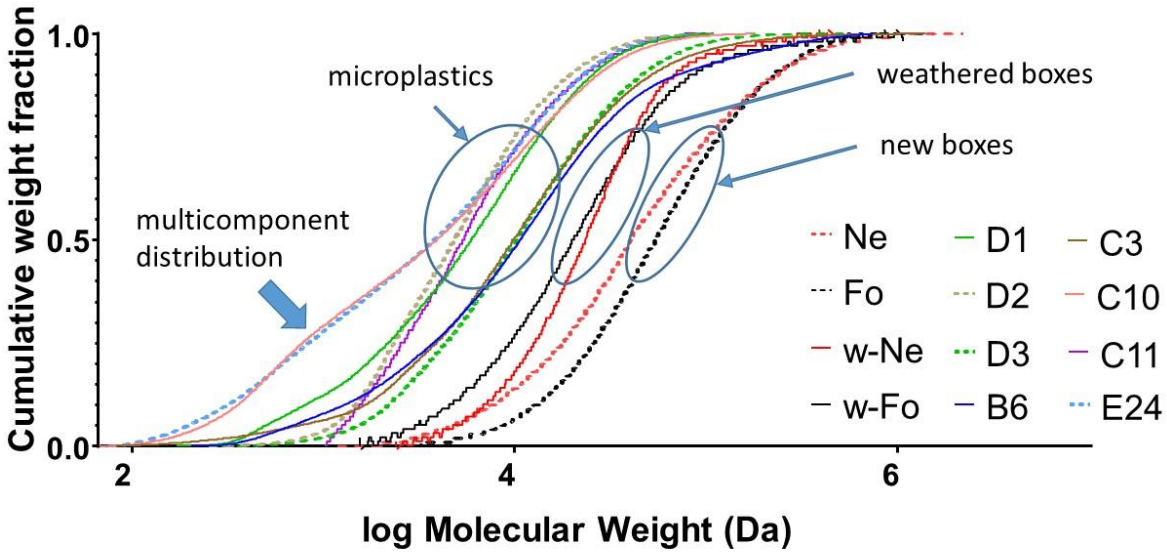

Fig. 2: Cumulative weight fraction showing the mass distribution of the polymer chains in the different samples.

The cumulative mass distributions shown in Fig. 2 indicate a strong decrease in molecular weight when the weathered boxes (w-Ne, w-Fo) are compared to the original ones (Ne, Fo). The micro-plastics present even lower molecular weights and their distribution tends to become multi-component, as can be seen from the tails in Fig. 2.

Table SI 3 summarizes the initial interpretation of the SE molecular weight distributions in terms of single and, in some cases, bimodal average values. Mn values are particularly low (below 5000

206 g.mol^{-1}) for all microplastics and their size distribution is better described by a multimodal
207 distribution, with average molecular weights Mn_1, Mn_2 and corresponding average degrees of
208 polymerisation, N_1, N_2. Microplastics E24, C11 and C10 have a mean Mn value close to 1000
209 g.mol^{-1}, indicating that they have, on average, smaller polymer chains than D1, D2, B6, C3 and
210 D3 microplastics. Macro or new materials have a significantly higher Mn value and longer polymer
211 chain lengths than the micro debris. The polydispersity index (PDI) is in general much larger for
212 microplastics. The statistical significance of these observations is shown in Fig. SI 2.

213

214 In conclusion, SEC shows a strong decrease of the polymer chain length between the original
215 packaging and the macroplastics. Interestingly, the size distributions of the microplastics are
216 usually multimodal. A spatially homogeneous scission would result in only a broadening of the
217 initial distribution. Here a spatially heterogeneous scission is most likely taking place. It could be
218 attributed to a preferred degradation at the surface (compared to the bulk) or related to selective
219 degradation in the semi-crystalline morphology (coexistence of crystalline and amorphous parts,
220 see Fig. 1) or a combination of both mechanisms.

221

222

DIFFERENTIAL SCANNING CALORIMETRY

DSC brings insights on: i) the kinetic arrest of PE crystallisation; and ii) the aging processes that altered the polymer organization (through the enthalpy of first fusion). Samples C8, D19 and E24 were too small to be characterized.

Fig. SI 3 shows typical DSC traces and the results of the statistical analysis are given in Table SI 4. The new boxes and macroplastics do not exhibit measureable differences whereas all microplastics have significantly higher crystallinity values (~70 %, on average, compared to ~50 % for macroplastics).

The melting can either be characterized by the peak position or at the beginning of the transition, *i.e.* the onset value (Table SI 4). No significant difference in the melting peak position was observed (Fig. SI 3). The onset temperatures were significantly lower for macro- compared to microplastics. The melting of the D1, B6 and C10 microplastics starts around 123-124°C. For the other microplastics, the fusion starts at higher temperatures: around 128°C for D2, C11 and C3; around 130°C for D3.

By comparing the SEC (Table SI 3) and DSC (Table SI 4) characterizations, it appears that the samples which are melting at lower temperatures (B6 and C10) exhibited the highest PDI. This is relevant with shortened chains being able to melt earlier. Moreover, the samples with the lower crystallinity exhibit a lower onset temperature of melting (macro versus micro samples). Owing to the very narrow distribution of the melting temperature between the microplastics (Fig SI 3), it is however impossible to compare SEC and DSC results more precisely. This is not surprising since physical properties are known to be poorly sensitive to molecular weight in these long chain polymers, contrary to small molecules and oligomers.[4]

WAXS

The radially averaged WAXS profile of Nesquik commercial packaging is shown In Fig. 3, along with the original 2D pattern (in the inset). Similar data are available for the other samples in Fig. SI 4. The WAXS patterns typically consist of many sharp and radially symmetric Debye-Scherrer rings and a single broad peak which is characteristic of the poorly defined interatomic distances of an amorphous solid.[23] The radial isotropy shows the lack of orientation expected from PE (powder pattern), along with a very limited number of spotty diffraction rings from filler or pigment material.

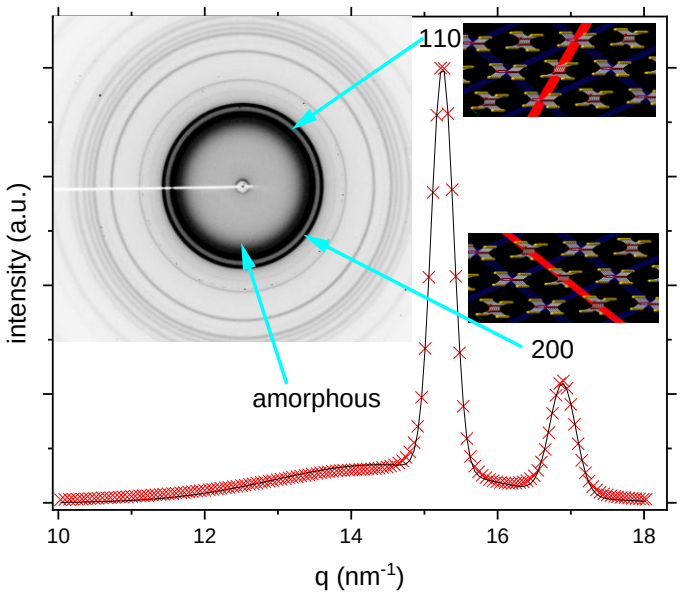

Fig. 3: Typical radially averaged WAXS data (red crosses) from Nesquik packaging material. Inset shows the corresponding 2D pattern. The black solid line shows the fit with three Gaussians described in the SI. Each lattice plane is shown in red on the cartoon next to the corresponding Bragg peak.

Using the crystal structure from Bruno et al.,[24] our analysis has focussed on the $10 < q < 18$ nm^{-1} q-range containing the 110 and 200 reflexions and the broad amorphous halo. There are numerous other peaks due to other less intense X-ray reflexions from PE and from the many

additives (e.g. colouring and fillers) which are found in commercial PE packaging.[25] The important fitted parameters are summarised in Table SI-5. From the FWHMs of the Bragg peaks (see Eqn's SI 3 and SI 4) we obtain the average coherence lengths D_{110} and D_{200} (see Fig. 1). The results of the analysis are given in Table 1. Crystallinities determined by WAXS and DSC are different but agree qualitatively (Figure SI-5). It is important to note that WAXS crystallinity is very sensitive to the data fitting procedure, and to the way the contributions of Bragg peaks are separated from the contribution of the amorphous peak.[26] This may explain that for all microplastics the values of the crystallinity derived from WAXS are overestimated compared to DSC.

The two average coherence lengths inside crystallite lamellae (D_{110} and D_{200} - Fig. 1) are significantly smaller for the microplastics than for the macroplastics (Table 1). For example, the value of D_{110} decreases in average value from 34 to 23 nm between macro and microplastics. The coherence length is defined as the extension of crystalline order normal to the specified crystallographic direction. We find that the in-plane crystalline order extends over a few tens of nanometres and decreases with weathering. Note here that the overall lateral size of the crystalline lamellae is expected to be much larger than the coherence length, typically of a few microns.[4] The in-plane order of the lamellae can be visualized as a collection of nano-sized crystalline domains. In conclusion, a higher crystallinity of these samples is associated to a smaller coherence length in the in-plane direction of the lamellae.

SAXS

In the semi-crystalline polymer model (Fig. 1) PE is organised in alternating lamellae of crystalline and amorphous polyethylene (PE) with electron densities, ρ_c and ρ_a , and thicknesses L_c and L_a, respectively. Because of this contrast in electron density, it is possible with SAXS to

measure the inter-lamellar spacing, called the long period L_P, with $L_P = L_c + L_a$. Fig. 4 shows the variation in 2D scattering patterns and the corresponding 1D SAXS profiles for different samples: Commercial Nesquik packaging (Ne), the corresponding weathered sample (w-Ne) and two microplastics (D19 and D1). All other SAXS patterns are given in Figure SI 6. As with WAXS, all the SAXS patterns are isotropic, and there is no preferential orientation of the lamellar structure. We will thus restrict the following discussion to the radially averaged 1D data.

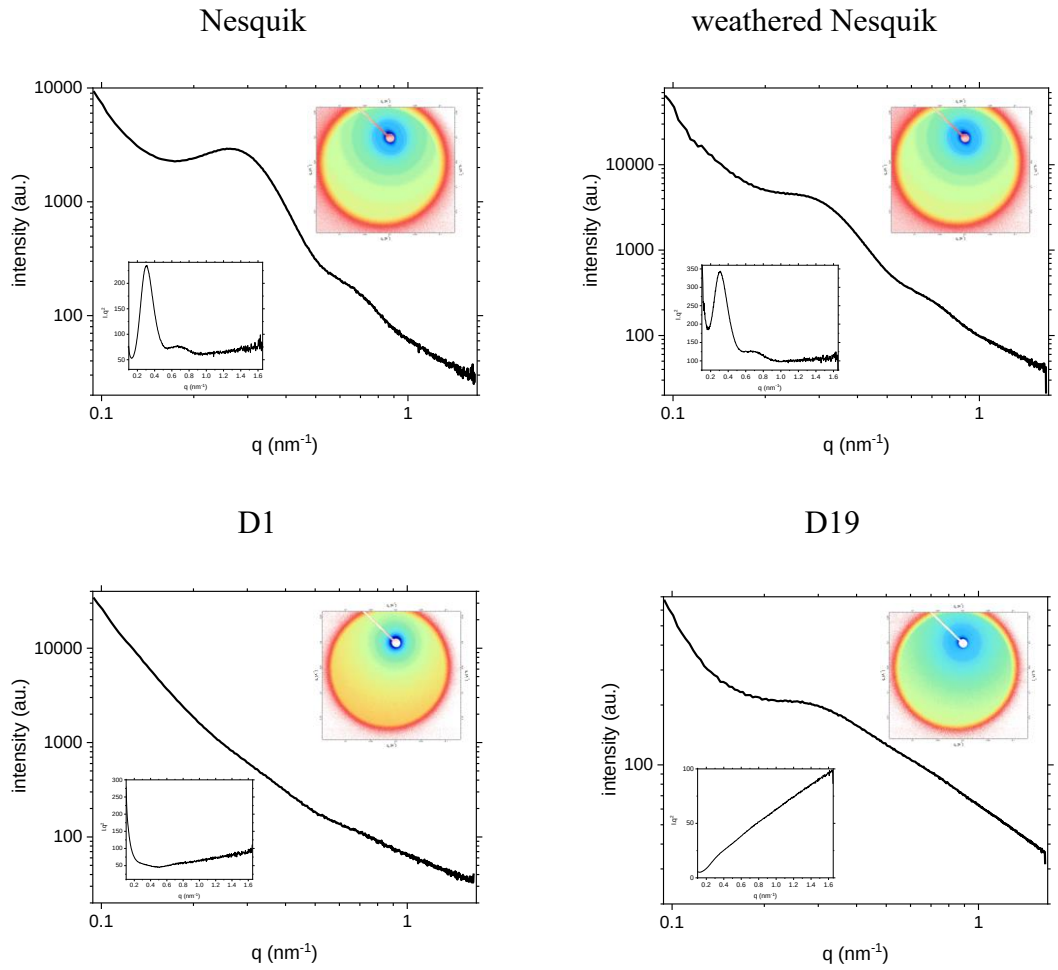

Fig. 4: Typical SAXS 1D profiles, with the corresponding 2D images (top right hand side insets) and Lorentz transformed data (bottom left hand side insets).

The intensity of the broad lamellar peak exhibits strong variations depending on the sample (Fig. 4 and Fig. SI 6). Generally, the raw packaging materials (Ne and Fo) have the most obvious peak.

The weathered macro debris (w-Ne and w-Fo) have a slightly less obvious feature. The microplastics exhibit either a very weak lamellar peak (D13 and C11), or no peak at all (C3, C10 and E24). Importantly, despite not exhibiting ordered lamellae, these samples do not exhibit any strongly different DSC crystallinities compared to the other samples in the same group: packaging; macroplastics; and microplastics. An exception is E24, the only sample that has no lamellar peak and a low crystallinity, comparable to that of the macroplastics.

The position of the peak in reciprocal space, q_{max}, may be converted to the real space lamellar spacing:

$$L_P = \frac{2\pi}{q_{max}} \quad (4)$$

The very broad SAXS peak is superimposed upon a sloping background. A convenient way of visualising the position of q_{max} is the Lorentz plot[27] - $q^2.I(q)$ (shown for the four spectra of Figure 4).

In order to estimate the linear crystallinity ($linC=L_c/(L_a+L_c)$) from those samples exhibiting a clear lamellar diffraction feature, we applied a cosine transform to the Lorentz transformed data. We thus obtained the linear correlation function ($\gamma_1(x)$), which maximum corresponds to L_c.[6]:

$$\gamma_1(x) = \frac{\int_0^\infty I(q)q^2 \cos(qx)dq}{\int_0^\infty I(q)q^2 dq} \quad (5)$$

The values obtained from the Lorentz plot and the subsequently cosine transformed data were consistent but the transform method was not suitable for those samples which exhibited very weak features. The SAXS plot for sample C8 was truncated by the limited solid angle of the 2D SAXS detector and it was difficult to extrapolate the high-q behaviour. The distributions of the L_P for samples that exhibit diffraction feature and/or were amenable to transformation to $\gamma_1(x)$ are shown in Fig. SI 7 and reported in Table 1. The value of L_P is rather constant for all samples, with L_P

close to 20 nm. According to Mann-Whitney test, no significant difference between the macro- and microplastics is observed.

The values of linC are higher than the values obtained from DSC and WAXS measurements (Fig. SI 5), with linC values close to 80% instead of 50% for the macroplastics. This difference if generally rationalised by considering that the value obtained for linC is not sensitive to the amorphous material outside the semicrystalline lamellae.[4]WAXS analysis does not rely on the assumption of a lamellar structure whereas SAXS analysis does and some samples could consist of bulk amorphous regions outside lamellae. In Table 1, last column, by proportional subtraction of values of linC from the overall crystallinity (determined by DSC), we estimate the amount of lamellar regions inside the material, in coexistence with extra amorphous regions.

In conclusion, unlike previous studies on PE samples with a well-defined environmental history,[6] we do not observe change or growth of L_P. Moreover, for microplastics, the long period peak in SAXS is not present or has a very weak intensity. A clear trend to the disruption of the lamellar order in the microplastics is observed.

RAMAN SPECTROSCOPY

Fig. 5a presents the low frequency Raman spectra collected from the samples and Fig. 5b gives the normalised linear thickness distributions (LTD) calculated from the mathematically adjusted LAM mode (Eqn.'s 2 and 3). Note that the fitted LAM position did not systematically match the apparent one in the raw spectrum. This points the importance of a spectral treatment to correct for the filtering-induced distortion, for superimposing contributions (mostly Rayleigh diffusion wing) and for the difficulty to set Raman shift origin precisely on the laser wavenumber with a pixel width ~ 0.5 cm^{-1} (see discussion in SI).

All the fitted LAM positions and corresponding L values ($L_{SCS\text{-}avg}$) are given in Table SI 6, as well as the most probable L value ($L_{SCS\text{-}mp}$) and the FWHM retrieved from each LTD (see SI). As a consequence of the distribution asymmetry, the most probable L_{SCS} is systematically about 2 nm below the average value.

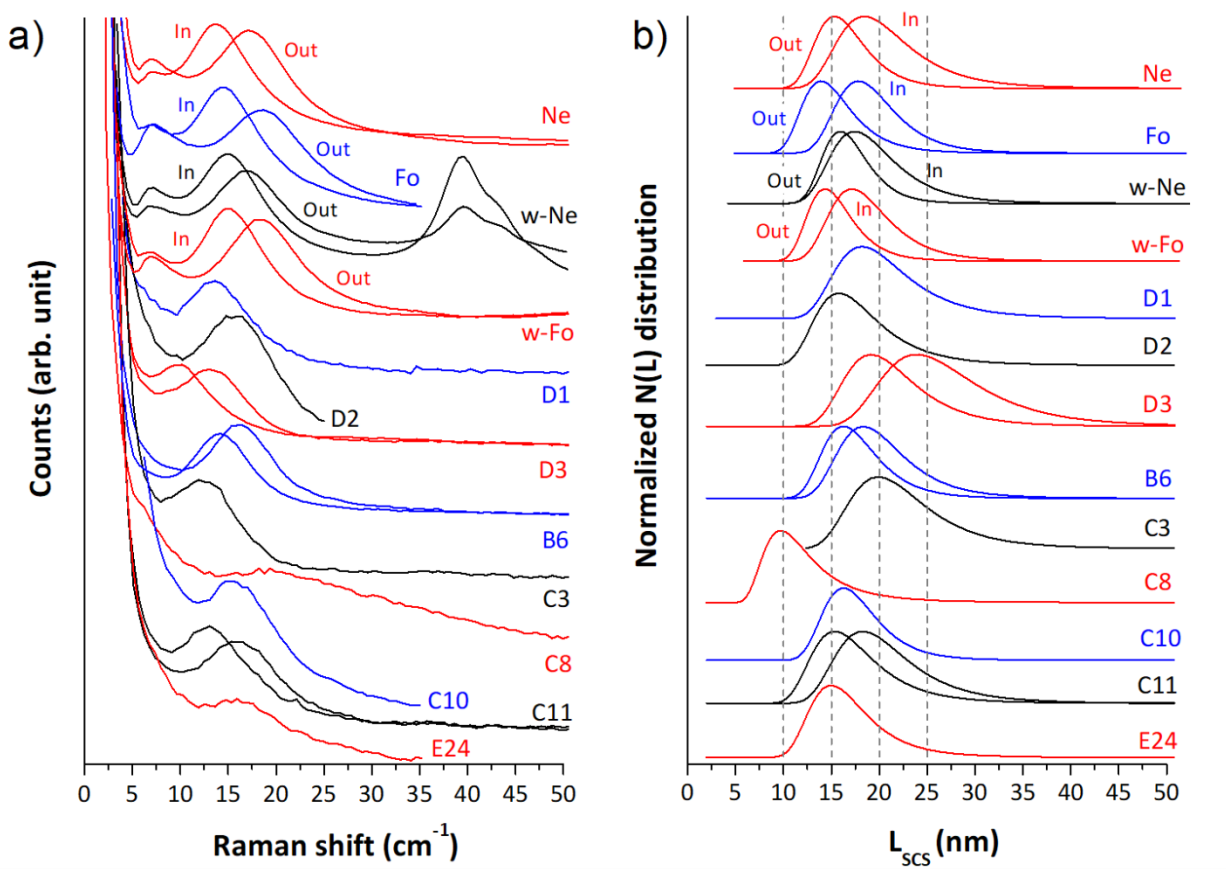

Fig. 5: (**a**) Low frequency Raman spectra corrected for the Rayleigh filtering stage (see SI); two spectra are given when distinct populations were observed depending on the point of analysis; In/Out labels specify which packaging wall was analysed; spectra from samples Fo, D2, C10 and E24 were truncated for clarity (**b**) L_{SCS} number distribution obtained from the fitted LAM profile (see Eqns 2 and 3 and SI).

The SCSs may be at an angle with the normal to PE lamellae but the average tilt is usually low enough (~35°)23-26 to still consider LSCS a good estimate for the lamellar thickness. As a matter of fact, the excellent agreement observed between the LSCS-mp

values obtained from low frequency Raman spectroscopy and LC values derived from SAXS (Table 1), while not specifically investigated here, is suggestive of a relatively low tilt angle in our samples.

The SCSs may be at an angle with the normal to PE lamellae but the average tilt is low enough (~35°)[7-10] to consider L_{SCS} a good estimate for the lamellar thickness. There is a small but systematic difference between the L_{SCS-mp} values obtained from low frequency Raman spectroscopy and L_C values derived from SAXS (Table 1), while not specifically investigated here, is suggestive of a relatively low tilt angle. Yet, SAXS results are averaged over the entire thickness of the samples whereas the penetration depth of Raman spectroscopy (a few micrometers below the surface, see SI) makes it possible to evidence structural differences between the inner and outer walls of the Folgers and Nesquik samples, without the need for sample sectioning. Besides, the Raman method is able to give a clear indication of the crystalline lamellar thickness when this is not possible for SAXS measurements, i.e. there is no SAXS diffraction feature.

The LTD is systematically increased by about 4 nm in the inner wall compared with the outer one (Tables 1 and SI 6). This is the first time, to our knowledge, that an inside vs. outside difference has been characterized in the literature on commercial PE packaging. This difference most probably results from a temperature gradient during the blow-moulding process. For those microplastics that reveal a two-mode distribution (D3, B6 and C11 samples) we might infer they corresponded to the inner and outer walls of the original packaging.

The direct comparison between a pristine and weathered sample of either Nesquik or Folgers packaging would obviously be questionable since they may not come from the same manufacturer or batch (see Fig 5(a) the ~40 cm^{-1} contribution that is detected in w-Ne but not observed in Ne sample). Yet, the general impression given by Fig. 5b and the Raman derived parameters from

Table SI 6 is that most $L_{SCS\text{-}mp}$ values stand in the ~15-20 nm range and that no systematic evolution of the LTD can be evidenced going from the pristine PE samples to weathered macroplastics and, ultimately, microplastics. The two outlier distributions are also the less reliable ones: C8 sample had very diffuse Raman scattering and the lowest peaks from D3 sample were at the ~10 cm^{-1} detection limit (Fig. SI 8a).

Table 1. Summary of the experimental results: **(i)** SEC-derived average number of monomer units per chain for monomodal (N) or bimodal (N_1 and N_2) size distributions (see Table SI 3 for details); **(ii)** DSC- and WAXS-derived crystallinity; **(iii)** WAXS-derived D_{110} and D_{200} coherence lengths; **(iv)** SAXS-derived values of the long period (L_P), the linear crystallinity (linC) and $L_C = L_p$*linC; **(v)** Raman-derived most probable L_{SCS} value; **(vi)** Estimation of the amount of lamellar phase (lam phase, %) in coexistence with extra amorphous regions; #: sample not analysed; *: irrelevant data.

Sample	N (N_1, N_2) SEC	Cryst. (%) DSC	Cryst. (%) WAXS	D_{110} (nm) WAXS	D_{200} (nm) WAXS	L_P (nm) SAXS	LinC (%) SAXS	L_C (nm) SAXS	L_{SCS-mp} (nm) Raman	Lam phase (%)
Probed vol.	1 mg	mm^3	mm^3	mm^3	mm^3	mm^3	mm^3	mm^3	μm^3	
Ne	721	53	53	33.8	28.4	20.2	78	15.8	15.4 – 18.5 (outer - inner)	68
Fo	1046	45	49	34.7	29.7	20.5	76	15.6	13.9 – 17.8 (outer - inner)	62
w-Ne	546	51	49	34.7	26.5	20.0	82	16.4	15.8 – 17.5 (outer – inner)	61
w-Fo	386	50	58	24.0	19.5	19.5	79	15.4	14.4 – 17.2 (outer – inner)	68
D1	82	64	74	23.1	20.8	no peak	*	*	18.2	*
D2	111 (418/68)	72	76	23.6	20.8	19.8	*	*	16.0	*
D3	186 (386/61)	69	77	23.1	21.1	23	*	*	19.1 – 24.2 (2 populations)	*
D19	#	*	72	22.7	20.8	18.2	89	16.2	#	81
B6	125 (179/9)	64	75	22.7	20.5	19.5	84	16.4	16.0 – 18.4 (2 populations)	83
C3	139 (357/27)	71	77	34.7	32.0	no peak	*	*	19.9	*
C8	#	*	74	23.1	20.8	8.3	76	6.3	9.7	97
C10	39 (189/14)	60	73	22.3	20.5	no peak	*	*	16.5	*
C11	36	72	77	23.6	21.1	18.5	*	*	15.5 – 18.4 (2 populations)	*
E24	34 (193/12)	#	52	23.6	19.2	no peak	*	*	15.0	*

To date most studies on the degradation of polyethylene have focussed on the chemical changes as a result of various interactions with light, the atmosphere and mechanical processes.[28] The dominant chemical reactions during degradation are polymer chain scission and/or oxidation. While ultimately degradation must be considered as a chemical process, physical changes in the solid state packing of polymer molecules have long been acknowledged as important determinant in the ability of many polymers to resist chemical and environmental degradation.[29] Furthermore, the scission of polymer chains by photodegradation has the effect of allowing polymer chains in kinetic arrest to adopt the lowest energy configuration and to crystallise further[6], which implies a clear link between chemical and physical changes.

A first objective of this work was to compare macroplastics (w-Ne and w-Fo samples) with their corresponding new packaging (Ne and Fo samples). What we observe is that although both samples undergo a reduction in molecular weight of PE, the sample with the greatest reduction in molecular weight (Fo to w-Fo) is the one that shows the greatest changes in nanostructure. Increase in crystallinity and decrease in the coherence length inside the crystalline lamellae are the two changes observed in this macroplastic. This trend is amplified for most microplastics. Importantly, all microplastics have much smaller molecular weight. As already known, scission of the polymer chains is the main chemical evolution that is taking place. We assert that this process underpins all the physical changes in the material. While macroplastics have crystallinities around 50 %, crystallinity in the microplastics is around 70 %, on average. This can be understood by the release of kinetic arrest to crystallization when polymer chains become shorter.

At the same time, Raman and SAXS do not evidence any systematic increase of the thickness of the crystalline lamellae, L_c and L_{SCS} always being close to 16 nm. This is quite surprising, as one would expect that increase in crystallinity should induce thickening of the crystalline lamellae,

with crystallisation occurring specifically at the crystalline/amorphous interface between lamellae, as was observed for PE systems exposed to specific doses of UV light.[6] In addition, the lamellar order is disappearing in most of the microplastics, as the peak related to the long period L_P is very weak or absent. Figure 6 is a cartoon summarising the evolution in the nanoscale structure: increase of the crystallinity and disruption of the lamellar order are taking place simultaneously.

Lastly, it will be important for future studies to take into account the structural heterogeneities of the original samples. It is well evidenced in Raman spectroscopy, with differences in the crystalline lamellar thickness L_{SCS} between the inside and outside surfaces of the packaging boxes. To date the effect of lamellar thickness on the crack resistance of PE has been investigated indirectly but would seem to be important.[30] There is also an open question regarding the heterogeneous scission of the PE chains evidenced by SEC measurements, most clearly in the microplastics. The resulting bimodal molecular weight distributions could be attributed to a preferred degradation at the surface (compared to the bulk) or related to selective scission inside crystalline versus amorphous PE.

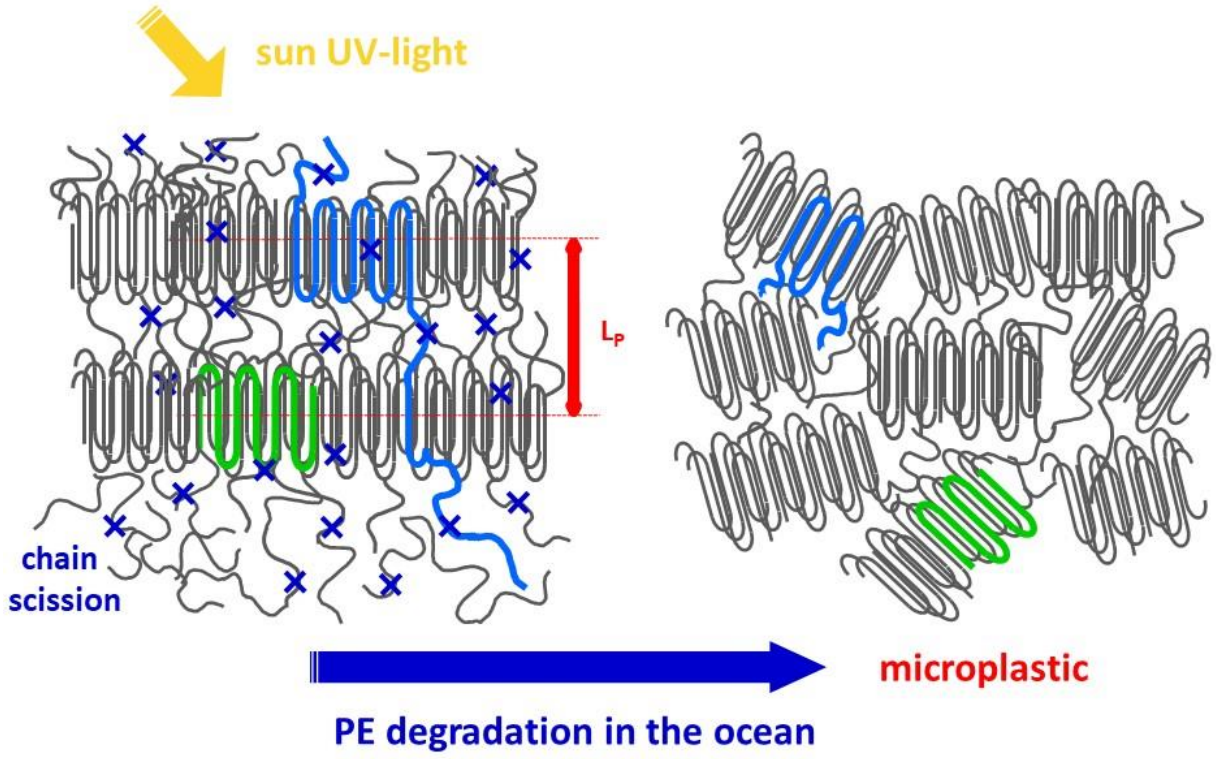

Figure 6. Summary of the observed evolution of semi-crystalline PE submitted to environmental conditions. Chain scission (indicated by blue crosses) induces a strong decrease of the average chain length (blue chains) and two main structural changes: increase in crystallinity and disruption of the lamellar order. In addition, no significant change in the thickness of the lamellae is observed and coherence lengths are slightly smaller (green crystalline domains). On the bottom part of the macroplastics scheme, possible coexistence of lamellar regions with extra amorphous regions is not depicted.

While the structural conclusions of this work are clear for each of the samples we have examined here, to directly relate these changes to the long-term effects of physical aging in the marine environment, is more difficult. In the case where the linage of aged samples can be clearly established, macro samples and commercial packaging, we observe clear changes in the polymerisation degree of PE. Chain scission can been induced by exposure to high-energy radiation or photochemical degradation, and similar changes in crystallinity and subsequent embrittlement were observed.[31-33] In the case of exposure to high energy radiation there is

substantial time lag (years) between the initial exposure/chain scission event and the full realisation of the structural changes.[33] Studies on degradation in model aquatic and marine systems have concluded that the effects of chemical degradation (oxidation) are causing both chain depolymerisation[34] and mass loss[35], which are associated with embrittlement of the bulk material on a shorter time scale. Though in the latter study[35] there was no explicit examination of the changes in molecular weight. Thus, radiation-induced chain scission and chemical degradation are both likely to occur in the marine environment, but on rather different timescales and with quite different impacts on the bulk and surface degradation of PE particles.

The important structural conclusion of this study is the loss of ordered semi-crystalline lamellar structure in aged microplastics. The arrangements of the lamellae provide a barrier to the diffusion of gases into the bulk polymer.[36] Assuming the crystalline regions present a barrier to diffusion of oxidants (most importantly oxygen) into PE the loss of the lamellar structure shown in Fig. 6 would allow freer chemical degradation with time. We therefore suggest that this important physical change in the arrangement of PE may enhance further chemical degradation of PE.

ASSOCIATED CONTENT

Supporting Information.

SI-file-PE-paper - January XXth

AUTHOR INFORMATION

Corresponding Authors

*Christopher J. Garvey: Lund Institute for Advanced Neutron and X-ray Scattering, Lund, Sweden; and Biofilm—Research Center for Biointerfaces and Biomedical Science Department, Faculty of Health and Society, Malmö University, Malmö, Sweden. Email: christopher.garvey@mau.se

Alexandra ter Halle: Laboratoire des IMRCP, Université de Toulouse, CNRS UMR 5623, Université Paul Sabatier, 118, route de Narbonne, F-31062 Toulouse Cedex 09, France. Email : ter-halle@chimie.ups-tlse.fr

Present Addresses

†

1. Lund Institute for Advanced Neutron and X-ray Scattering, Lund, Sweden
2. Department of Biomedical Science, Malmö University, Malmö, Sweden

Author Contributions

The manuscript was written through contributions of all authors. All authors have given approval to the final version of the manuscript.

ACKNOWLEDGMENT

C.G. acknowledges the CNRS and Université Paris-Sud for financial support during his sabbaticals.

This project is supported by the Total Corporate Foundation and The French National Research Program for Environmental and Occupational Health of Anses (EST/2017/1/219).

ABBREVIATIONS

DSC, differential scanning calorimetry; FWHM, Full Width at Half Maximum; LAM, Longitudinal acoustic mode (Raman spectroscopy); linC, linear crystallinity; LTD, Lamellar Thickness Distribution; PDI, polydispersity index; PE, polyethylene; SAXS, small angle X-ray scattering; SEC, Size exclusion chromatography; WAXS, wide angle X-ray scattering.

REFERENCES

1. Geyer, R.; Jambeck, J. R.; Law, K. L., Production, use, and fate of all plastics ever made. *Science Advances* **2017,** *3* (7).
2. Jambeck, J. R.; Geyer, R.; Wilcox, C.; Siegler, T. R.; Perryman, M.; Andrady, A.; Narayan, R.; Law, K. L., Plastic waste inputs from land into the ocean. *Science* **2015,** *347* (6223), 768-771.
3. Lucas, N.; Bienaime, C.; Belloy, C.; Queneudec, M.; Silvestre, F.; Nava-Saucedo, J. E., Polymer biodegradation: Mechanisms and estimation techniques. *Chemosphere* **2008,** *73* (4), 429-442.
4. Strobl, G. R., *The Physics of Polymers: Concepts for Understanding Their Structures and Behavior*. Springer: 2007.
5. Hsu, Y. C.; Truss, R. W.; Laycock, B.; Weir, M. P.; Nicholson, T. M.; Garvey, C. J.; Halley, P. J., The effect of comonomer concentration and distribution on the photo-oxidative degradation of linear low density polyethylene films. *Polymer* **2017,** *119*, 66-75.
6. Hsu, Y. C.; Weir, M. P.; Truss, R. W.; Garvey, C. J.; Nicholson, T. M.; Halley, P. J., A fundamental study on photo-oxidative degradation of linear low density polyethylene films at embrittlement. *Polymer* **2012,** *53* (12), 2385-2393.
7. Bassett, D. C.; Hodge, A. M.; Olley, R. H.; Keller, A., On the morphology of melt-crystallized polyethylene - II. Lamellae and their crystallization conditions. **1981,** *377* (1768), 39-60.
8. Voigt-Martin, I. G.; Mandelkern, L., A quantitative electron microscopic study of the crystallite structure of molecular weight fractions of linear polyethylene. *Journal of Polymer Science: Polymer Physics Edition* **1984,** *22* (11), 1901-1917.

9. de Silva, D. S. M.; Zeng, X.-b.; Ungar, G.; Spells, S. J., On Perpendicular and Tilted Chains in Lamellar Crystals. *Journal of Macromolecular Science, Part B* **2003,** *42* (3-4), 915-927.
10. Fritzsching, K. J.; Mao, K.; Schmidt-Rohr, K., Avoidance of Density Anomalies as a Structural Principle for Semicrystalline Polymers: The Importance of Chain Ends and Chain Tilt. *Macromolecules* **2017,** *50* (4), 1521-1540.
11. ter Halle, A.; Ladirat, L.; Gendre, X.; Goudouneche, D.; Pusineri, C.; Routaboul, C.; Tenailleau, C.; Duployer, B.; Perez, E., Understanding the Fragmentation Pattern of Marine Plastic Debris. *Environmental Science & Technology* **2016,** *50* (11), 5668-5675.
12. ter Halle, A.; Ladirat, L.; Martignac, M.; Mingotaud, A. F.; Boyron, O.; Perez, E., To what extent are microplastics from the open ocean weathered? *Environmental Pollution* **2017,** *227*, 167-174.
13. Ilavsky, J., Nika: software for two-dimensional data reduction. *J. Appl. Crystallogr.* **2012,** *45* (2), 324-328.
14. Mizushima, S.-i.; Simanouti, T., Raman Frequencies of n-Paraffin Molecules. *Journal of the American Chemical Society* **1949,** *71* (4), 1320-1324.
15. Snyder, R. G.; Krause, S. J.; Scherer, J. R., Determination of the distribution of straight-chain segment lengths in crystalline polyethylene from the Raman LAM-1 band. *Journal of Polymer Science: Polymer Physics Edition* **1978,** *16* (9), 1593-1609.
16. Blackadder, D. A.; Lewell, P. A., The density of polyethylene single crystals. *Polymer* **1968,** *9*, 249-263.
17. Palmö, K.; Krimm, S., Chain elastic modulus of polyethylene: A spectroscopically determined force field (SDFF) study. *Journal of Polymer Science Part B: Polymer Physics* **1996,** *34* (1), 37-45.
18. Wassermann, T. N.; Thelemann, J.; Zielke, P.; Suhm, M. A., The stiffness of a fully stretched polyethylene chain: A Raman jet spectroscopy extrapolation. **2009,** *131* (16), 161108.
19. Snyder, R. G.; Strauss, H. L.; Alamo, R.; Mandelkern, L., Chain-Length Dependence of Interlayer Interaction In Crystalline N-Alkanes From Raman Longitudinal Acoustic Mode Measurements. *Journal of Chemical Physics* **1994,** *100* (8), 5422-5431.
20. Lüttschwager, N. O. B.; Suhm, M. A., Stretching and folding of 2-nanometer hydrocarbon rods. *Soft Matter* **2014,** *10* (27), 4885-4901.
21. Snyder, R. G.; Scherer, J. R., Interpretation of longitudinal-acoustical-mode spectra of polymers. *Journal of Polymer Science: Polymer Physics Edition* **1980,** *18* (3), 421-428.
22. Samuel, A. Z.; Hamaguchi, H.-o., A General Approach for Estimating Lamella-Thickness Distribution in Polymers with Low-Frequency Raman Spectroscopy: Application to Lamella Formation in Crystallizing Polyethylene. **2018,** *24* (37), 9333-9339.
23. Guinier, A., *X-ray diffraction: in crystals, imperfect crystals, and amorphous bodies*. Dover publications: 1994.
24. Bruno, J. A. O.; Allan, N. L.; Barron, T. H. K.; Turner, A. D., Thermal expansion of polymers: Mechanisms in orthorhombic polyethylene. *Phys. Rev. B* **1998,** *58* (13), 8416-8427.
25. Tolinski, M., *Additives for Polyolefins: Getting the Most out of Polypropylene, Polyethylene and TPO*. Elsevier Science: 2015.
26. Klug, H. P. A., *X-Ray Diffraction Procedures - For Polycrystalline and Amorphous Materials*. Wiley: 1954.

27. Cser, F., About the Lorentz correction used in the interpretation of small angle X-ray scattering data of semicrystalline polymers. *Journal of Applied Polymer Science* **2001,** *80* (12), 2300-2308.
28. Singh, B.; Sharma, N., Mechanistic implications of plastic degradation. *Polymer Degradation and Stability* **2008,** *93* (3), 561-584.
29. Krässig, H. A., *Cellulose: Structure, Accessibility, and Reactivity*. CRC Press Inc: 1993.
30. Fodor, J. S.; Lamborn, M. J.; DesLauriers, P. J., Correlating polyethylene microstructure to stress cracking: Development of primary structure parameters. *Polymer* **2018,** *147*, 8-19.
31. Fayolle, B.; Colin, X.; Audouin, L.; Verdu, J., Mechanism of degradation induced embrittlement in polyethylene. *Polymer Degradation and Stability* **2007,** *92* (2), 231-238.
32. Fayolle, B.; Richaud, E.; Colin, X.; Verdu, J., Review: degradation-induced embrittlement in semi-crystalline polymers having their amorphous phase in rubbery state. *Journal of Materials Science* **2008,** *43* (22), 6999-7012.
33. Bhateja, S. K., Radiation-induced crystallinity changes in linear polyethylene: Influence of aging. *Journal of Applied Polymer Science* **1983,** *28* (2), 861-872.
34. Colin, X.; Audouin, L.; Verdu, J.; Rozental-Evesque, M.; Rabaud, B.; Martin, F.; Bourgine, F., Aging of Polyethylene Pipes Transporting Drinking Water Disinfected by Chlorine Dioxide. I. Chemical Aspects. *Polym Eng Sci* **2009,** *49* (7), 1429-1437.
35. Da Costa, J. P.; Nunes, A. R.; Santos, P. S. M.; Girao, A. V.; Duarte, A. C.; Rocha-Santos, T., Degradation of polyethylene microplastics in seawater: Insights into the environmental degradation of polymers. *J. Environ. Sci. Health Part A-Toxic/Hazard. Subst. Environ. Eng.* **2018,** *53* (9), 866-875.
36. Eby, R. K., Diffusion in polymer with lamellar morphology polyethylene. *Journal of Applied Physics* **1964,** *35* (9), 2720-&.